Rarefied-Flow Aerodynamics and Thermosphere Structure from Shuttle Flight Measurements

Robert C. Blanchard* and Gregory M. Buck†
NASA Langley Research Center, Hampton, Virginia

This report presents the flight data results from the High Resolution Accelerometer Package (HiRAP) experiment on the sixth and seventh shuttle missions (i.e., STS-6 and STS-7). The data have been reduced to produce aerodynamic force coefficients, principally L/D in the rarefied flow regime. Also, a technique is used to extract approximate body-axis aerodynamic coefficients from the flight data. Comparisons of the rarefied transition flow aerodynamic behavior between the two sets of flight data indicate differences, primarily in the free-molecule flow coefficients; i.e., STS-7 shows a free-molecule flow behavior that correlates with diffuse surface reflection conditions, while STS-6 does not. The data have also been used to estimate the density profiles in the upper atmosphere. The atmospheric density is generated from 60 to 160 km from each flight. The density profiles produced have a primary wave structure and differences are observed between the two sets of flight data. A new rarefied transitional flow aerodynamic bridging formula has been generated from the flight data. Comparisons with the flight bridging formula and existing Monte Carlo and wind-tunnel data are made.

Nomenclature

A_x, A_z	= measured accelerations in the x and z channels
C	= aerodynamic coefficient
$\bar{C}$	= normalized transition aerodynamic coefficient, $(C-C_C)/(C_F-C_C)$; $0<\bar{C}<1$
C_A	= axial force coefficient
C_R	= drag coefficient
C_N	= normal force coefficient
Kn	= Knudsen number
ℓ	= lag parameter
L/D	= lift-to-drag ratio
L_D	= vehicle reference length
M	= Mach number
$\bar{M}$	= mean molecular weight
N/A	= normal-to-axial force ratio
R	= A_z/A_x ratio
RE	= Reynolds number
S/M	= spacecraft area to mass ratio
v	= spacecraft velocity
$\bar{V}_\infty$	= modified viscous parameter
α	= angle of attack
δ	= deflection angle
λ	= atmosphere mean free path
ρ	= mass density

Subscripts

C	= hypersonic continuum flow regime
BF	= body flap
EL	= elevon
F	= free molecule flow regime
ℓ	= determined from the lag model
0	= at $Kn=10^{-3}$
p	= predicted value
62	= from the 1962 standard atmosphere

Submitted Nov. 20, 1984; presented as Paper 85-0347 at the AIAA 23rd Aerospace Sciences Meeting; Reno, NV, Jan. 14-17, 1985; revision received April 20, 1985. This paper is declared a work of the U.S. Government and therefore is in the public domain.

*Entry Data Group Leader, Aerothermodynamics Branch, Space Systems Division. Member AIAA.

†Aerospace Engineer, Aerothermodynamics Branch, Space Systems Division. Member AIAA.

Introduction

HIGH-resolution (i.e., micro-g) accelerometer data from the HiRAP experiment have been obtained on all Shuttle Orbiter Vehicle OV-099 and OV-102 flights starting with the sixth Orbiter flight. The preliminary results from the initial flight of the HiRAP and a description of the processing technique required to extract the aerodynamic accelerations from the measured re-entry signals have been reported earlier.[1] Additional analysis of the STS-6 data and the complete analysis of STS-7 data are summarized and discussed in this paper.

Data from the HiRAP experiment provide information on the aerodynamic force coefficients at rarefied flow transitional conditions. These data for a winged entry vehicle, such as the Orbiter, are not readily obtainable in the wind tunnel where, for a variety of reasons, it is difficult to produce direct measurements on models at the combined low Reynolds numbers and large Mach numbers. Also, current computational methods[2] cannot provide the force coefficients for a lifting entry vehicle like the Orbiter because of computational limitations. That is, in principle, the Monte Carlo technique can provide force data, but the storage capacity and program running time are prohibitive with reasonable cell size resolution and vehicle geometry. Hence, designers who need transitional flow regime aerodynamic data have resorted to empirical representations based mostly upon sparse flight data from past programs, such as Apollo.[3] This situation is now being remedied by the repeated Orbiter flights with the HiRAP, which are providing a large body of rarefied flow flight data with some variation of flight conditions.

Both accelerometer and atmospheric measurements are required to obtain aerodynamic force coefficient information from flight data.[4] The long-range experiment plan is to provide atmospheric density data with a mass spectrometer system especially adapted to the Orbiter as a separate experiment.[5] However, for the early flights of the HiRAP equipment, the mass spectrometer is not available. Thus, assumptions on atmospheric density are necessary for obtaining the individual aerodynamic force coefficients, e.g., C_A and C_N. However, an atmospheric assumption for the ratio of force coefficients, e.g., C_N/C_A, is not required since dynamic pressure cancels in the formation of the ratio. But, even for force ratio measurements, some estimates of atmospheric parameters are necessary in order to identify the flow regime or to calculate the associated scaling parameters, such as Knudsen number.

In this paper, the individual force components and density will be addressed in the following manner. First, the preflight data book normal force coefficient will be assumed. This allows density to be calculated from accelerometer flight data along the normal axis. The density results will be compared with the 1962 standard atmosphere.[6] Second, this derived atmosphere will be used in combination with the axial channel accelerometer measurements to calculate the axial force coefficient. The results will be compared with the preflight predicitions. As a final step, an approximate relationship between the normal and axial coefficients is made in order to derive independent force coefficients from the accelerometer flight data. The basis for this total approach is that the normal coefficient undergoes relatively small changes as the vehicle passes through the transitional-flow flight regime, thus providing a means of obtaining the in situ density to a good approximation. That is, under this assumption, the HiRAP can also provide density measurements at altitudes in which little measurements exist, namely, above the threshold of conventional sounding devices and below satellite observation altitudes.

Analysis of Flight Data

Correlation with Trajectory Parameters

Time-tagged HiRAP data at 174 samples/s are recorded during the re-entry of the Orbiter starting about 10 minutes prior to deorbit burn and continuing until after touchdown when the instrument and recorder are turned off. During this data acquisition period, other data are also taken and used to obtain the best estimated trajectory (BET). The process and technique of obtaining the BET has been reported earlier.[7]

The HiRAP raw flight data are reduced to engineering units by the application of calibration factors. The aerodynamic acceleration signal is then extracted with a postflight processing technique[1] which includes removal of thrust, removal of linear accelerations due to rotation of sensors offset from the center of gravity, and the application of a smoothing procedure. The aerodynamic acceleration data are then merged with the BET results, in particular the velocity, angle of attack, and altitude parameters, as well as the Inertial Measurement Unit (IMU) data. The IMU contains a separate triad of accelerometers used by the Orbiter for onboard navigation and guidance. The merging consists of linearly interpolating the trajectory parameters to each HiRAP data point since the BET and HiRAP are not recorded at the same data rate and are not synchronized to each other. The IMU data, used to generate the BET, characterize the vehicle behavior near the continuum regime when HiRAP channels saturate. Calibration and corrections for off center-of-gravity rotational motions are done in the generation of the BET, and no further manipulations are necessary except time correlation with the HiRAP data.

Force Ratio Measurements

An important step in obtaining information about the rarefied-flow aerodynamics from acceleration measurements is the evaluation of the ratio A_z/A_x since atmospherics is not a direct factor. For this experiment, the ratio is a measure of C_N/C_A, or equivalently N/A, since the input axes of the accelerometer triad are accurately aligned with the vehicle body axes. Figure 1 shows the force ratio measurements in the body axes coordinate system for STS-6 and STS-7. The HiRAP flight measurements are above 97 km, while the IMU measurements are below. The graph of the data depicts the anticipated behavior of the aerodynamics as the vehicle flies through the rarefied-flow transition regime. That is, in the free-molecule flow regime, at high altitudes, the ratio is about 1.0. As the boundary layer thickens upon re-entry, the shear forces become progressively less significant, causing the ratio to approach large values; for this vehicle the hypersonic continuum force ratio is about 18. Typically, between the altitudes shown, the vehicle aerodynamics "transitions" from hypersonic continuum coefficients at the lower altitudes to free-molecule flow coefficients at the higher altitudes. This approximate regime for the orbiter is indicated at the top of the figure.

These body axes can be transformed to the familiar wind axis system, using angle of attack α, obtained from the onboard navigation gyro data which are also recorded during reentry. The transformation of the data is

$$L/D = (R - \tan\alpha)/(1 + R\tan\alpha)$$

The data period of interest is after the Orbiter has achieved its nominal fixed re-entry attitude of 40-deg angle of attack. This is typically about 10 min prior to the arbitrary entry interface mark of 121.92 km (400,000 ft). Thus, for this study the flight regime of interest is from about 160 km down to about 60 km. This covers as much of the rarefied-flow regime at fixed angle of attack as possible with a significant overlap into the hypersonic continuum regime. Figure 2 shows the detailed altitude profile of the measured α throughout the region of interest for both flights being studied.

Figure 3 shows the results of the calculations of the L/D for STS-6 and STS-7. Again, the figures are composed of two sets of data from different instrumentation. Data from the HiRAP at high altitudes (above about 97 km) are shown with data from the IMU providing the remaining portion of the curve into the hypersonic continuum regime. The behavior of STS-6 data is about the same as the preliminary presentation discussed in Ref. 1. However, the free-molecule flow L/D appears considerably lower on STS-7 than on STS-6. Further

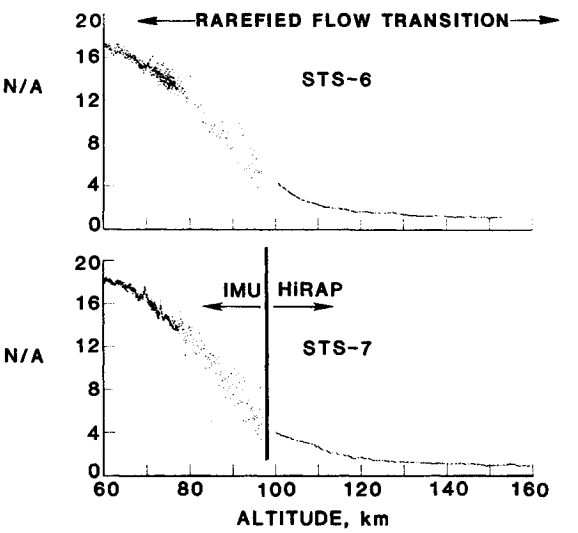

Fig. 1 *N/A* measurements in the rarefied flow regime.

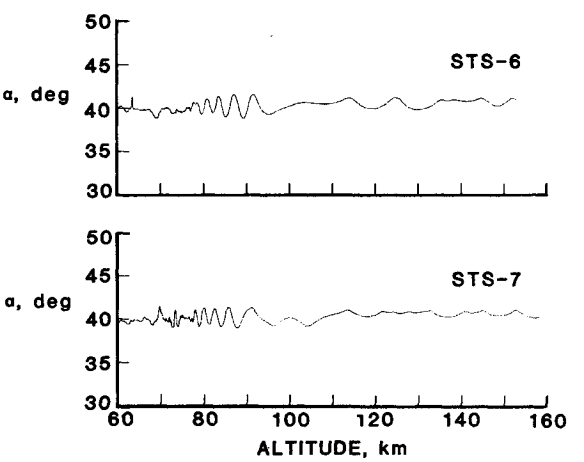

Fig. 2 Angle-of-attack measurements from the IMU.

calculations indicate that the average value of free molecule flow data shown is very near the predicted value for complete energy accommodation, i.e., $L/D=0.04$, indicated by the dashed line labeled "diffuse." Diagnostic indicators from instrumentation systems show that the hardware was functioning within normal limits on both missions. Thus, either the vehicle has changed surface reflection characteristics after its first entry, or there is a substantial difference in the atmospheric properties between each flight. That is, on STS-7, the atmosphere is less dense and the vehicle is well into the free-molecule flow regime at 160 km, while for STS-6 at 160 km, the atmosphere is more dense and, thus, the vehicle is already in the transition flow regime. Since there are no direct measures of atmospheric properties, it is only possible to infer the more likely solution to the observed differences between the flights.

Atmosphere Calculations

The principal atmospheric state component affecting the accelerometers is mass density. As mentioned earlier, separation of density from accelerometer measurements requires information on the aerodynamic coefficients. For this study, the generation of density profiles for each flight assumed the accepted flight values of the hypersonic continuum normal force coefficients[8] and the data book values of the free-molecule flow normal force coefficient.[9] Normal force coefficients were chosen because it is anticipated that the variation through the transitional flow regime is relatively small compared to the axial force coefficient. That is, the vast shear force change shows up mostly in C_A for this configuration. The density profiles shown as Fig. 4 for both flights included the following calculation:

$$\rho = -2\,A_Z/v^2 C_{N_p}(S/M)$$

where v^2 is obtained from the BET.

The data shown in Fig. 4 are from two instrument systems (HiRAP and IMU), and density in mormalized with respect to the 1962 standard. Clearly evident in both flights are the atmospheric phenomena reported earlier in Ref. 1, namely, a waveform of large proportion, about 50 to 60% magnitude superimposed on the standard. However, on the STS-7 flight the wave is about 10 to 15 km higher and thus is sensed almost entirely by the HiRAP instument. Also, there is a significant difference in density between the flights at 160 km. This shift corresponds to an expanded upper atmosphere or a more rarefied condition at a fixed altitude, which may well account for the observed differences in L/D between the two flights. For instance, if the inferred atmosphere shown on Fig. 4 were accepted, then the corresponding Knudsen number for STS-6 at 160 km would be only 4.1, while for STS-7 it would be 23.0 at the same attitude. Thus, it could be argued that the larger value of L/D for STS-6 is the result of the vehicle's residing in the transitional flow regime. Of course, it is not possible to be definitive since C_N is assumed in these density calculations and

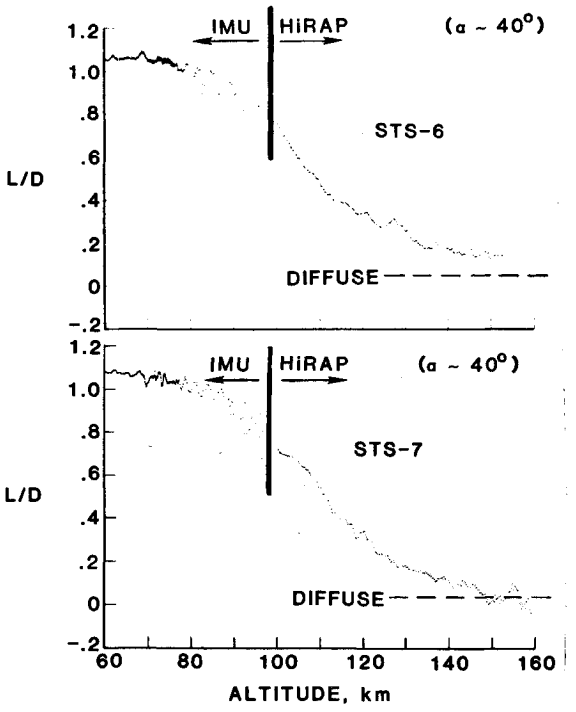

Fig. 3 L/D measurements in the rarefied flow regime.

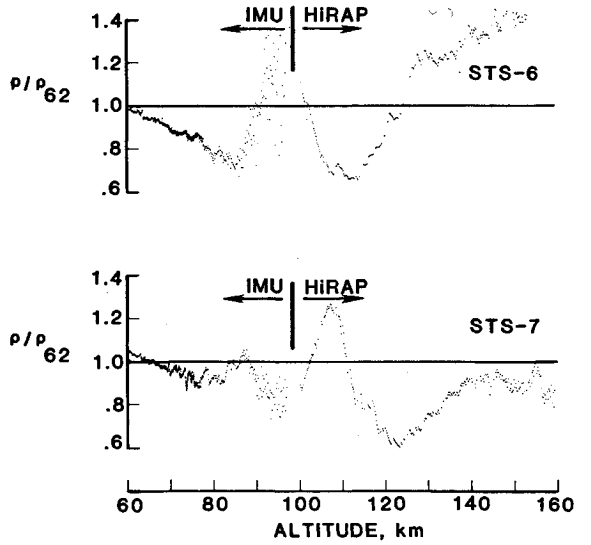

Fig. 4 Normalized density profiles inferred from accelerometry.

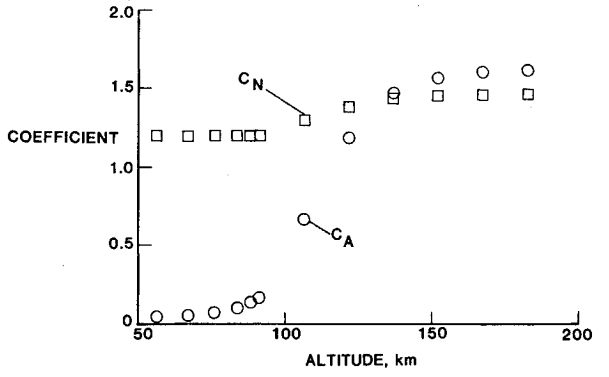

Fig. 5 Aero data book preflight coefficients for zero control surface deflections; $\alpha = 40$ deg.

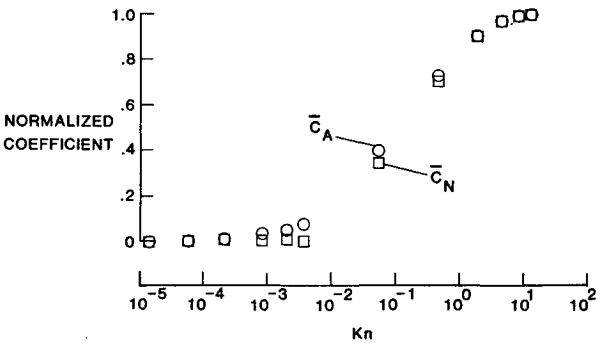

Fig. 6 Normalized aero data book preflight coefficients.

it is based upon diffuse reflection data book assumptions. It is quite clear from this figure that a disturbance appears on both flights. Although it is seen that the altitude location of the disturbance is different on each flight, there is no obvious aerodynamic phenomenon that could produce the variations observed on each flight such that it exactly cancels in the ratio. Therefore, it is concluded that the disturbance is atmospheric in origin, perhaps, due to gravity waves as described by Hines.[10]

Body Axes Force Coefficients

Predicted Coefficients

The occurrence of the wave structure on two flights has prompted additional investigations into the individual measurement channels, principally x and z. The predicted variation with altitude, based on the 1962 standard atmosphere, of both coefficients is displayed in Fig. 5. The predictions are for a constant angle of attack of 40 deg and control surfaces of 0 deg. These data are from the orbiter design data book, which is a compendium of aerodynamics information based upon many contributors in wind tunnels, flow computation, etc., taken during the orbiter's development. Notice on the figure that from the free-molecule flow to the hypersonic continuum regime, C_N varies about 17%, corresponding mostly to a change in pressure force, while C_A undergoes a change of a about 96%, reflecting mostly the vast change in shear forces mentioned previously. For this report, it is useful to normalize the coefficients in studying their behavior in the transition regime. Figure 6 is a graph of the result of this normalization plotted against Knudsen number. The predicted coefficients are based upon a Kn with reference length of 12.0609 m (39.57 ft), which is the orbiter's mean chord length. This scaling parameter is used thoughout in order to compare the flight results directly to the predictions. Above a Knudsen number of $Kn = 10^{-3}$, the data book values are based on the $\sin^2\omega$ term as used in the following bridging formulas.

$$C_A = C_{A_0} + (C_{A_{FM}} - C_{A_0})\sin^2\omega$$

$$C_N = C_{N_0} + (C_{N_{FM}} - C_{N_0})\sin^2\omega$$

$$\omega = \pi(3 + \log_{10} Kn)/8$$

where C_{A_0} and C_{N_0} are experimentally available at the Knudsen number $Kn = 10^{-3}$. At lower values of Kn, below 10^{-3}, the normalized data book values in Fig. 6 represent actual wind-tunnel data. Note on the graph that the axial coefficient leads the normal coefficient in rising toward the free-molecule flow regime, due to viscous effects. The normal coefficient lag is accomplished in the data book by separately merging the same $\sin^2\omega$ term into the near hypersonic continuum coefficients. At the free-molecule flow extreme, the $\sin^2\omega$ function is tied at the same boundary, namely, $Kn = 10$.

Flight Component Derived Coefficients

The same atmosphere component must necessarily appear in each channel since the same density affects the separate channels proportionately. The inverse calculations of the preceding section have been performed. That is, assuming the density derived from the normal coefficients, the axial force coefficient is calculated using

$$C_A = -2\,A_x/v^2\rho(S/M)$$

The Kn variation is also obtained using the flight-derived density and the following approximation with mean molecular weight $\bar{M}$ obtained from a 1962 standard atmosphere. That is,

$$Kn = \lambda/L_D \simeq 2.8\times 10^{-9}(\bar{M}/\rho L_D)$$

The flight-derived normalized axial coefficient is obtained from

$$\bar{C}_A = (C_A - C_{A_C})/(C_{A_F} - C_{A_C})$$

where C_{A_C} and C_{A_F} are the hypersonic continuum and free-molecule flow values for a given α, δ_{EL}, and δ_{BF}, respectively. The hypersonic continuum values used in this analysis are from previous flight assessments,[8] while the free-molecule values are from the data book,[9] which is based upon theoretical calculation using diffuse surface reflection conditions.

Axial Coefficient Comparisons

Figure 7 shows the results of the $\bar{C}_A$ calculations as a function of Kn for STS-6. The preflight data book values for the normalized axial and normal coefficient are also presented on the same graph. Note the difference in the normalized flight axial coefficient and the data book axial coefficient, suggesting that some improvements can be made. Near the continuum, the flight data and the empirical formula agree somewhat, mostly due to the arbitrary tie-down of the bridging formula. Also, the data book C_N curve lies above flight-derived C_A, which does not follow preflight expectations. Thus, an approximate relation between the axial and normal coefficient is required. This approximation can be achieved by adjusting the C_N, which is discussed next.

Normal Coefficient Approximation

The manner by which the normal coefficient is approximated makes use of the lag parameter ℓ, defined as the multiplicative factor by which the scaling parameter Kn lags in value between equivalent C_A and C_N measurements. That is, $\log_{10}(\ell)$ is the amount by which a curve through C_A is shifted to the right along the $\log_{10}(Kn)$ axis. The value for ℓ used is 2.8, which is the ratio of the square root of the projected normal-to-axial areas of the Orbiter. This value of ℓ accounts

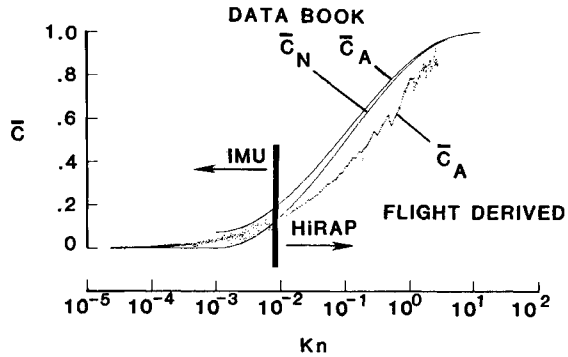

Fig. 7 Comparison of STS-6 flight-derived axial coefficients with predicted coefficients.

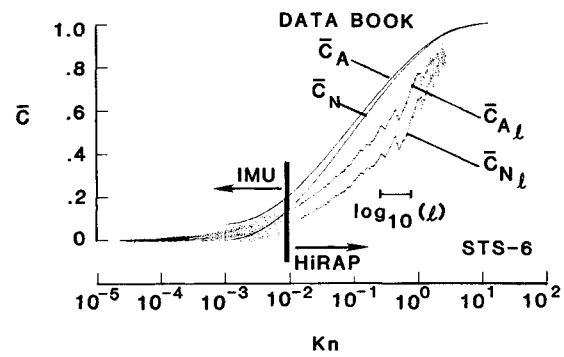

Fig. 8 Comparison of STS-6 coefficients from flight accelerometry ($\ell = 2.8$) with predicted coefficients.

approximately for relative differences in the degree of rarefaction in the individual aerodynamic components due to different cross-sectional areas of the vehicle.

Using an iterative procedure to calculate corresponding axial and normal coefficients that satisfy the lag requirement ℓ, along with a related density, the values C_{A_ℓ}, C_{N_ℓ}, and ρ_ℓ are determined directly from the accelerometer flight data. The calculation results for STS-6 of C_{A_ℓ} and C_{N_ℓ}, are shown in Fig. 8 with the corresponding data book predicted values. C_{A_ℓ}, varies only slightly from C_A obtained originally, although now the normal coefficient C_{N_ℓ} is in a desired relation with respect to the axial coefficient. The corresponding change in density calculations from the previously derived density is represented in Fig. 9 as the ratio of the two densities. Note that only a 5% change in density is involved in the adjustment of the flight coefficient relationships. This change in density does not substantially change any of the figures or conclusions stated previously.

It is interesting to note the behavior of the coefficients when $\log_{10}(\ell) = 0$. Figure 10 is a graph of the results of these calculations. Here the normalized axial and normal coefficients are set equal, and the curve is very near the values of C_A and C_{A_ℓ} calculated previously, indicating the insensitivity of the calculated axial force coefficient in relation to changes in C_N.

Flight-Derived Bridging Formula

General problems have become evident in applications of the $\sin^2\omega$ bridging formula provided by the current data book. Specifically, a problem arises when the bridging formula is used as the data book prescribes for predicting axial force coefficients. Through midtransition and toward the free-molecule end of transition, the data book formula represents a smooth curve similar in both C_N and C_A coefficients. However, toward the continuum flow regime, the bridging formula ties into the continuum value for the normal force coefficient but matches only partway there for the axial coefficient, and from thereon a different functional model (and scaling parameter) is used. At the point of matching between the two data book functions for C_A, a major slope or attachment discontinuity occurs using flight-derived scaling parameters. This makes it an unlikely and awkward model of aerodynamic force variations in that particular flight regime. Further, the bridging formula did not follow the behavior of the flight data in the transitional flow regime as discussed above. These behavioral differences may be due to choice of scaling parameter or other factors. But for comparative reasons with flight data results, it is worth investigating a separate formulation.

A new bridging formula was designed to overcome the above-mentioned difficulties. This formula is based on the previous calculations for $\bar{C}_A$ using STS-6 and STS-7 flight data and is given as

$$Z = \exp[A|B - \log_{10}Kn|^C]$$

where $A = -0.2553$, $B = 1.073$, and $C = 1.850$. The normalized axial coefficient is then given by

$$\bar{C}_A = Z(Kn)$$

An approximation for a normal-force coefficient can be given using the same empirical curve. To accomplish this requires shifting the empirical Z function above, similar to that done in the data book model. However, unlike the data book boundary value approach, the shift is accomplished by using an adjusted Knudsen number relation to match existing preflight tunnel data for near continuum flow properties. These existing data show constant values for C_N at Knudsen numbers from about 10^{-5} to 0.002. Mathematically this constraint can be met using the empirical Z function and a "lag" parameter, $\ell = 2.8$, which is equivalent to the projected area ratio previously described. This approach utilizes the exponentially increasing nature of the new bridging formula to approximate a constant C_N at the lower Knudsen number values. Thus, similar to the C_A curve representation, the normal coefficient variation is given as

$$\bar{C}_N = Z(Kn/\ell)$$

This transitional formula for the normal force coefficient is offered for completeness when modeling aerodynamics with the revised flight bridging formula and is as valid a first-order approximation of C_N variation as the data book model.

Figure 11 is the comparison of the new bridging formula with the flight data from the STS-6 and STS-7 HiRAP and IMU. As seen, the curve satisfactorily encompasses the flight data from the HiRAP through transition. For the ordinate scale shown, the IMU flight data virtually lay on top of the curve in the viscous regime at small Knudsen numbers. Thus, the function behaves through transition and well into the hypersonic continuum. Finally, the flight-derived bridging formula provides an easier mechanism to compare the flight data with other data sources. This is discussed next.

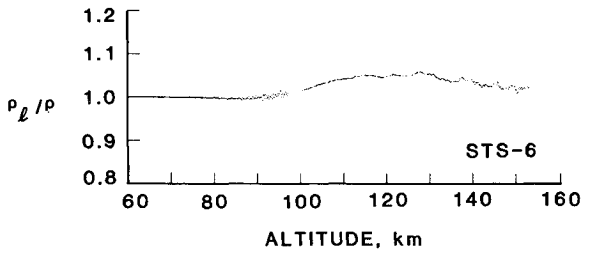

Fig. 9 Ratio of derived densities for flight STS-6.

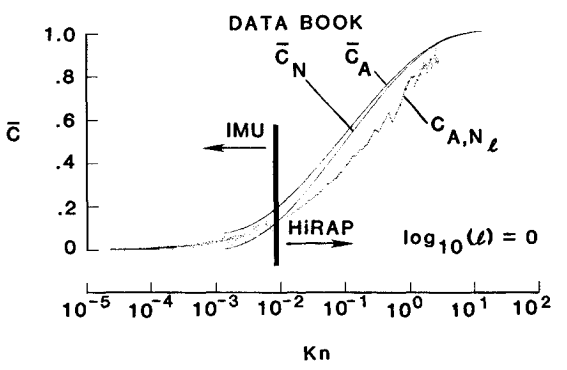

Fig. 10 Comparison of STS-6 combined coefficients ($\ell = 1$) with predicted coefficients.

Flight Bridging Formula Comparisons

Monte Carlo Data

A comparison of the flight-derived bridging formula with flowfield drag results obtained by Moss and Bird using the direct simulation Monte Carlo (DSMC) method has been made.[2] The model used in the DSMC calculations is a hyperboloid that closely approximates the Orbiter nose region but is different from the total flight vehicle. However, the flight conditions on STS-6 and STS-7 closely match the transitional flow of the Monte Carlo study so that the drag curve presented in Ref. 2, when normalized, should provide a reasonable test for the new transition bridging formula and, thus, the flight data. To perform the comparisons, the normalized drag coefficient is calculated by

$$C_D = C_A\cos\alpha + C_N\sin\alpha$$

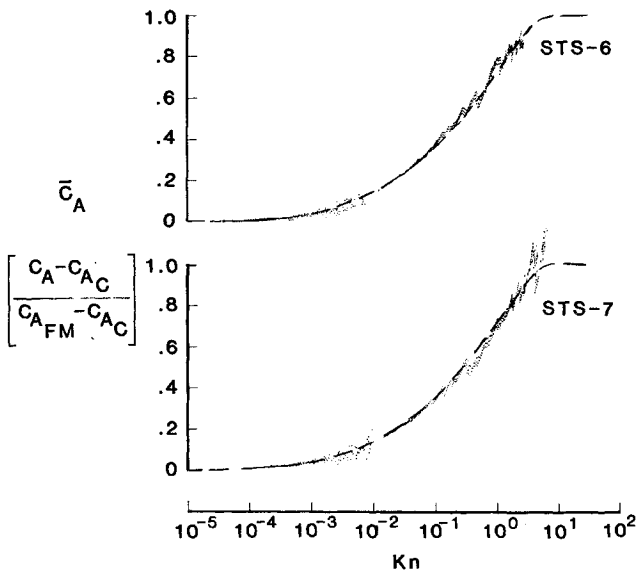

Fig. 11 Comparison of flight axial coefficient for STS-6 and STS-7 with flight-derived bridging formula.

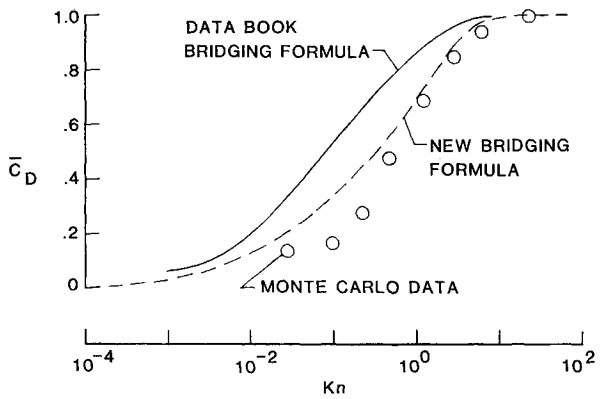

Fig. 12 Comparison of flight and data book transition bridging formula with Monte Carlo data.

and

$$\bar{C}_D = (C_D - C_{D_C})/(C_{D_F} - C_{D_C})$$

Figure 12 is a graph of the flight-derived and data book empirical bridging formula with the normalized Monte Carlo data, using the corresponding Knudsen number defined in Ref. 2. Near the free-molecule regime, i.e., large Knudsen numbers, there is good agreement with the flight-derived formula and the Monte Carlo simulation. However, the agreement departs as the hypersonic regime is approached, i.e., small Knudsen numbers. There are several potential reasons for this departure. First, the geometry model differences may yet be a factor. Second, perhaps the rarefaction parameter Kn is not the appropriate scaling parameter, although the DSMC calculations used freestream conditions based upon early shuttle flights.

Wind-Tunnel Data

Shuttle wind-tunnel test data have been obtained for hypersonic flow, $M = 10$ to 25, simulating vehicle aerodynamics for near-continuum flight conditions up to the fringes of rarefied transitional flow. These data were obtained during the formative period of the Shuttle program at various facilities throughout the country and documented in Ref. 11. Figure 13

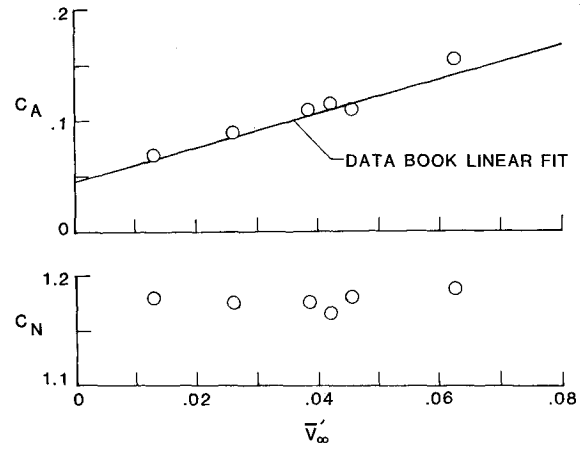

Fig. 13 Near continuum Calspan tunnel data, $\alpha = 40$ deg.

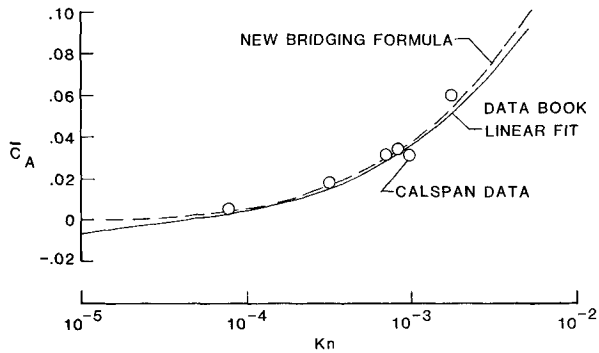

Fig. 14 Comparison of normalized axial tunnel data and linear fit with flight bridging formula.

is a plot of measured wind-tunnel force coefficients from Ref. 11 for angle of attack, $\alpha = 40$ deg, and includes the linear curve fit of C_A variation used in the current data book. For comparisons of these data with the present flight-derived bridging formula, an estimation of the $\bar{V}_\infty$ flight parameter is required. This is necessary since both the wind-tunnel data and its prediction curve fit are shown here and in the preflight data book as a function of this scaling parameter for near-continuum transition flow. The $\bar{V}_\infty$ variation, with respect to Kn, was obtained from the flight-derived density and atmosphere models defined by the 1962 standard. The wind-tunnel data and linear data book curve fit shown in Fig. 13 are transformed to normalized coefficients and shown again in Fig. 14 as a function of Kn for the axial coefficient. In this figure, the comparison is then made with the present bridging formula for $\bar{C}_A$.

There is good agreement between this bridging formula and the experimental ground data well into the hypersonic flight regime, at least to Kn values of about 10^{-4}. By extending through the near-continuum flow regime and being a function of a single rarefaction parameter Kn, this new bridging formula avoids the discontinuities that exist in the current data book model, which uses a linear representation with $\bar{V}_\infty$ below $\bar{V}\infty = 0.08$ and a $\sin^2\omega$ function of Knudsen number above 0.08.

Conclusion

Experimental flight data from the HiRAP accelerometers on STS-6 and STS-7 have been reduced and analyzed to produce flight rarefied aerodynamic force coefficients, principally L/D. At lower altitudes, less than 90 km, the IMU accelerometers are used and the aerodynamic coefficient results from both flights agree well. The flight data from STS-7 show

much lower L/D values in the free-molecule flow regime than STS-6. The near-diffuse surface reflection conditions on the second flight of the HiRAP are attributed either to changed vehicle surface properties due to previous re-entry or to the fact that the density of the upper atmosphere on STS-7 is substantially lower than for STS-6. Solving for atmospheric density with the flight data indicates that about a 50% change in density would resolve the issue since STS-6 would reside in the transitional flow regime where STS-7 would reside in the free-molecule flow regime.

Solving for the atmospheric density from the STS-7 flight data has again generated a density wave structure that was observed on STS-6. The wave is remarkably similar to the one derived from STS-6 except that the wave has shifted 10 to 15 km higher in altitude for STS-7. This shift is in agreement with a less dense atmosphere and serves as additional evidence for an atmospheric explanation for the observed L/D differences. The wave structure was also observed in both individual accelerometer channels at about the same level, thus pointing to an atmospheric phenomenon—possibly gravity waves—as the cause.

The absence of density measurements in the flight regime studied during each flight has prompted the development of a separate technique to extract individual force coefficients. The technique is based upon the observation that the normal force coefficient changes are relatively small over the complete rarefied transitional regime; estimates are about 17%. Thus, a good approximation of density variation can be obtained using the preflight normal force coefficient, along with the normal accelerometer flight data. This allows for the reasonable determination of the axial force coefficient. However, conversely, the normal coefficient is difficult to obtain due to its lack of sensitivity. But, for completeness, an approximation to the normal coefficient has been given by introducing a "lag" model based upon the ratio of the square root of the projected areas. This simple procedure probably accounts for the normal coefficient behavior to first order but is only an approximation based upon matching the available near-continuum tunnel results. Complete examination of rarefaction effects for this component of force must await the flight of the combined accelerometers (HiRAP) and the mass spectrometer (SUMS).

A new bridging formula was generated and compared with the data from STS-6 and STS-7. The suggested formula overcomes the data book bridging formula difficulties and agrees well with the newly acquired flight data and the shuttle experimental data base in the near-continuum regime and the Monte Carlo results in the near free-molecule flow regime. Although the formula has limited uses for the current STS, its utility lies in defining performance aerodynamics of future reentry missions, such as aero-assisted orbital transfer vehicles or the Entry Research Vehicle. This improvement may well prove important for missions that rely more on transitional flow aerodynamics than the shuttle does.

References

[1]Blanchard, R. C. and Rutherford, J. F., "The Shuttle Orbiter High Resolution Accelerometer Package: Preliminary Flight Results," *Journal of Spacecraft and Rockets,* Vol. 22, July-Aug. 1985.

[2]Moss, J. N. and Bird, G. A., "Direct Simulation of Transitional Flow for Hypersonic Reentry Conditions," AIAA Paper 84-0223, Jan. 1984.

[3]Wilhite, A. W., Arrington, J. P., and McCandless, R. S., "Performance Aerodynamics of Aero-Assisted Orbital Transfer Vehicle," AIAA Paper 84-0406, Jan. 1984.

[4]Blanchard, R. C. and Walberg, G. D., "Determination of the Hypersonic Continuum Rarefield Flow Drag Coefficient of the Viking Lander Capsule 1 Aeroshell for Flight Data," NASA TP 1973, Dec. 1980.

[5]Blanchard, R. C., Duckett, R. J., and Hinson, W. E., "The Shuttle Upper Atmosphere Mass Spectrometer Experiment," *Journal of Spacecraft and Rockets*, Vol. 21, March 1984, p. 202.

[6]*U.S. Standard Atmosphere,* 1962, NASA, USAF, USWB, Dec. 1962.

[7]Compton, H. R., Findlay, J. T., Kelly, G. M., and Heck, M. L., "Shuttle (STS-1) Entry Trajectory Reconstruction," AIAA Paper 81-2459, Nov. 1981.

[8]*Flight Assessment Package Orbiter Aerodynamics*, NASA JSC-19654, April 1984.

[9]*Aerodynamic Design Data Book—Volume I: Orbiter Vehicle*, NASA CR-160386, 1978.

[10]Hines, C.O., "Internal Atmospheric Gravity Waves at Ionospheric Heights," *Canadian Journal of Physics*, Vo. 38, 1960.

[11]*Aerodynamics Design Substantiation Report—Vol. I: Orbiter Vehicle,* Rockwell International, Space Division, SD74-SH-0206-1H, Jan. 1975.